ESI

Chiral probe development for circularly polarised luminescence: comparative study of structural factors determining the degree of induced CPL with four heptacoordinate europium(III) complexes

Emily R. Neil, Robert Pal, Lars-Olof Palsson, Benjamin A. O'Sullivan and David Parker*

Department of Chemistry, Durham University, South Road, Durham, DH1 3LE, UK

Email: david.parker@dur.ac.uk

General Experimental

Materials

All reagents were purchased and used as received. Analytical solvents were purchased from Fisher Scientific and were laboratory grade. Anhydrous solvents were freshly distilled over the appropriate drying agent and stored under argon in a septum-capped bottle. Water was purified by the 'Purite$_{STILL}$plus' system, with conductivity of ≤ 0.04 μS cm^{-1}. Air sensitive reactions were carried out under an atmosphere of argon using Schlenk-line techniques.

Analytical Methods

Thin layer chromatography was carried out on neutral aluminium silica plates (Merck 5554) or neutral aluminium oxide plates (Merck 5550) and visualised under UV irradiation (254/365 nm). Preparative column chromatography was performed using silica gel (Merck Silica Gel 60, 230-400 mesh) or neutral aluminium oxide (Merck 90, 70-320 mesh).

^{1}H and ^{13}C NMR spectra were recorded on a Varian Mercury-200 (^{1}H 199.975 and ^{13}C 50.289), Varian Mercury-400 (^{1}H 399.960 and ^{13}C 100.572), Bruker Avance-400 (^{1}H 400.052 and ^{13}C 100.603), Varian Inova-500 (^{1}H 499.722 and ^{13}C 125.671), Appleby VNMRS-600 (^{1}H 599.832 and ^{13}C 150.828), or Varian VNMRA-700 (^{1}H 699.731 and ^{13}C 175.948) spectrometer. Spectra were

recorded in commercially available deuterated solvents. ^{13}C and ^{1}H chemical shift values are quoted in ppm relative to trimethylsilane and all coupling constants are given in Hz. Assignment of the spectra was achieved using COSY, DEPT, HSQC and HMBC experiments. The operating temperature of the spectrometers (usually 295 K) was measured with the aid of an internal calibration solution of ethylene glycol. The operating temperature of each spectrometer was measured before each set of measurements of relaxation data, using the calibration sample.

Melting points were recorded using a Gallenkamp (Sanyo) apparatus and are uncorrected.

Electrospray mass spectra were recorded on a Thermo-Finnigan LTQ FT instrument operating in positive or negative ion mode as stated, with methanol or acetonitrile as the carrier solvent. Accurate mass spectra were recorded using the Thermo-Finnigan LTQ FT mass spectrometer. LCMS analyses were performed on a Waters system comprising a 3100 Mass Detector and a 2998 Photodiode array detector.

Reverse phase HPLC purification was performed at 295 K using a Shimadzu system consisting of a Degassing Unit (DGU-$20A_{5R}$), a Prominence Preparative Liquid Chromatograph (LC-20AP), a Prominence UV/Vis Detector (SPD-20A) and a Communications Bus Module (CBM-20A). An XBridge C18 OBD 19 x 100 mm, i.d. 5 μM column was used with a flow rate of 17 mL/min (prep). The solvent was H_2O + 0.1% formic acid / MeOH + 0.1% formic acid (gradient elution).

All samples for optical analyses were contained in quartz cuvettes with a path length of 1 cm and a polished base. Measurements were recorded at 295 K. UV/Vis absorbance spectra were recorded on a ATI Unicam UV/Vis spectrometer (Model UV2) using Vision version 3.33 software. Samples were measured relative to a reference of pure solvent contained in a matched cell. Emission spectra were recorded on an ISA Jobin-Yvon Spex Fluorolog-3 luminescence spectrometer using DataMax v2.2.10 software. Lifetime measurements were carried out on a Perkin Elmer LS55 spectrometer using FL Winlab software version 4.00.02.

CPL spectra (Fig. S1) were recorded on a custom built spectrometer consisting of a laser driven light source (Energetiq EQ-99 LDLS, spectral range 170 to 2100 nm) coupled to an Acton SP2150 monochromator (600 g/nm, 300 nm Blaze) that allows excitation wavelengths to be selected with a 6 nm FWHM band-pass. The collection of the emitted light was facilitated (90 º angle set up, 1 cm path length quartz cuvette) by a Lock-In Amplifier (Hinds Instruments Signaloc 2100) and Photoelastic Modulator (Hinds Instruments PEM-90). The differentiated light was focused onto an Acton SP2150 monochromator (1200 g/nm, 500 nm Blaze) equipped with a high sensitivity cooled Photo Multiplier Tube (Hamamatsu 7155-01 red corrected). Spectra were recorded using a 5 spectral average sequence in the range of 570-720 nm with 0.5 nm spectral intervals and 500 μs integration time. The recorded

CPL spectrum underwent a 25% Fourier transformation smoothening protocol using Origin 8.0 Software (Origin Labs) to enhance appearance (all calculations were carried out using raw spectral data).

Apparent binding constants were calculated by fitting equation 1.0 to emission data, using a non-linear least squares fitting algorithm in Microsoft Excel 2010, with the solver add-in.

$$[X] = \frac{\frac{(F - F_0)/(F_1 - F_0)}{K} + [Eu] * (F - F_0)/(F_1 - F_0) - [Eu] * \left[(F - F_0)/(F_1 - F_0)\right]^2}{1 - (F - F_0)/(F_1 - F_0)}$$

1.0

$$Eu + X \leftrightarrow EuX$$

$$K = \frac{[EuX]}{[X_f][Eu_f]}$$

[*X*]: Total concentration of the selected analyte in solution

[*Eu*]: Total concentration of the complex

K: Binding constant

F: Intensity ratio of selected peaks

*F*0: Initial ratio

*F*1: Final ratio

[*EuX*]: the concentration of the analyte-coordinated complex

[*X f*]: the concentration of free analyte in the mixture

[*Eu f*]: the concentration of the free complex

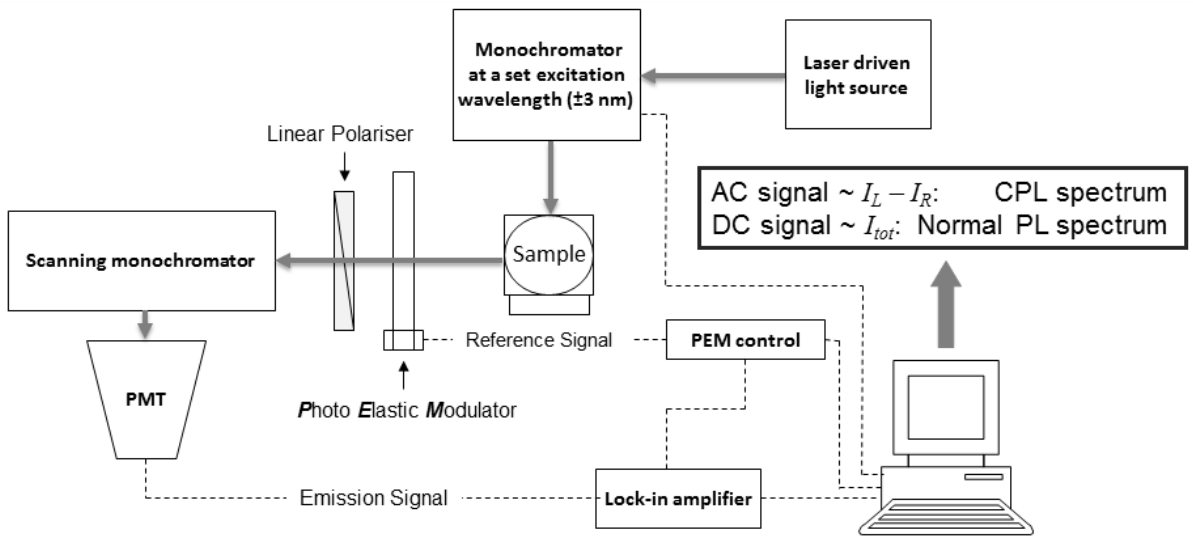

Figure S1 schematic diagram of Durham CPL instrumentation.

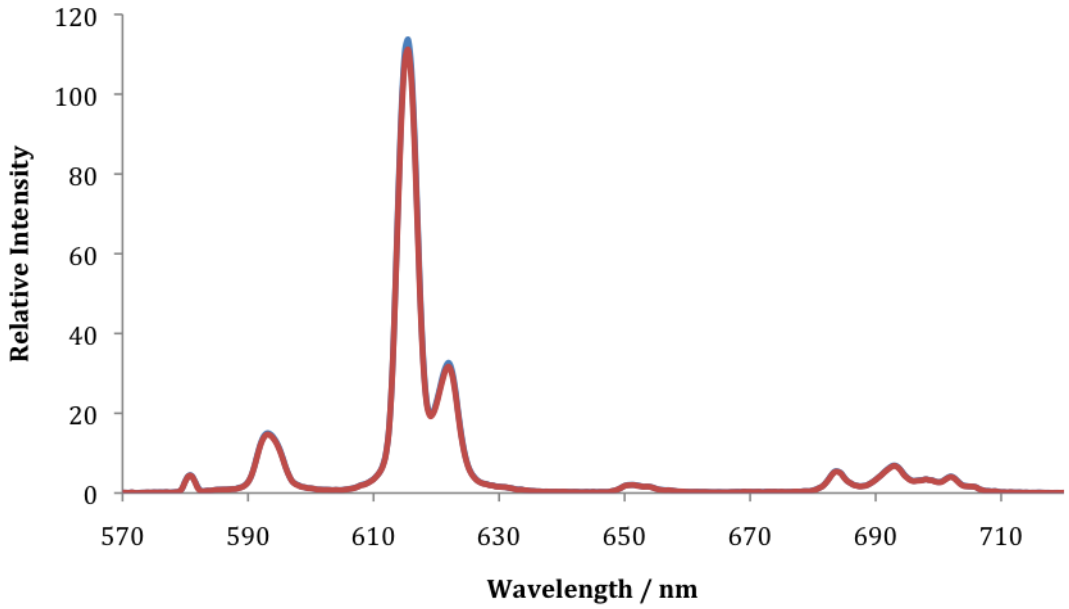

Figure S2a Emission spectra of [Eu.$\mathbf{L}^3$]$^+$ following the addition of a sample of 100% *R*-mandelate (blue) and 50% *R*-mandelate (red) (10 μM complex, λ_{exc} = 352 nm, MeOH). The correspondence is indicative of no significant variation with mandelate enantiomeric purity.

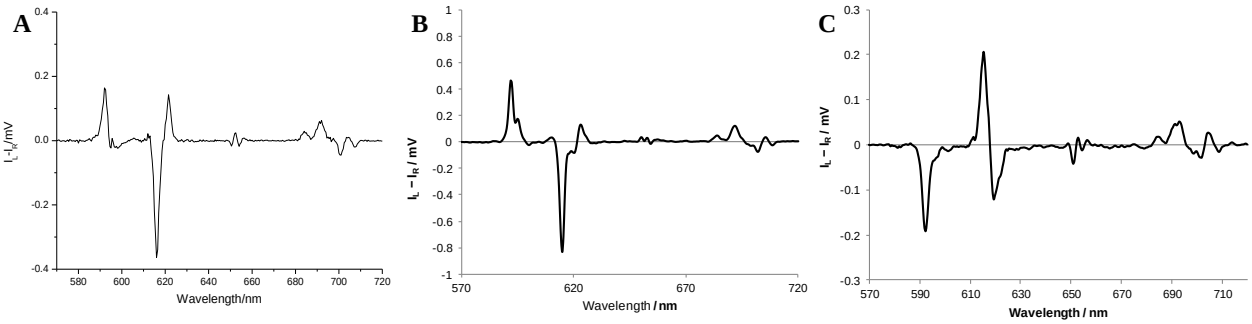

Figure S2b CPL spectra following addition of *R*-cyclohexylhydroxyacetate: (A) [Eu.$\mathbf{L}^{\mathbf{1}}$]$^{+}$; (B) [Eu.$\mathbf{L}^{\mathbf{3}}$]$^{+}$; (C) [Eu.$\mathbf{L}^{\mathbf{2}}$]$^{3+}$ (10 μM complex, MeOH, 295K), showing the common spectral fingerprint in the ΔJ = 4 region between 675 and 725 nm (see main text).

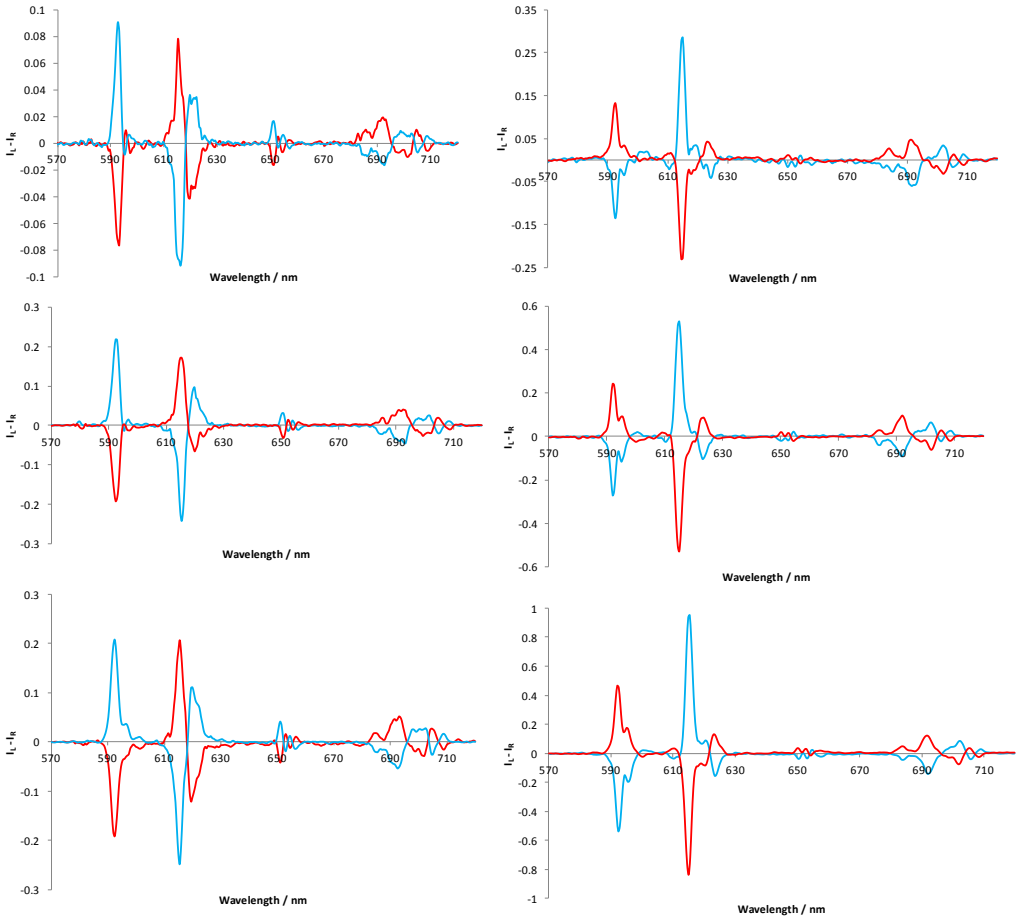

Figure S3 CPL spectra of [Eu.$\mathbf{L}^{\mathbf{2}}$]$^{3+}$ (*left*) (H_2O) and [Eu.$\mathbf{L}^{\mathbf{3}}$]$^{+}$ (*right*) (MeOH) on the addition of 2 mM *R*(red) and *S*(blue) lactate (*top*), mandelate (*centre*) and cyclohexylhydroxyacetate (*lower*) (10 μM complex, pH 5.5, 295K).

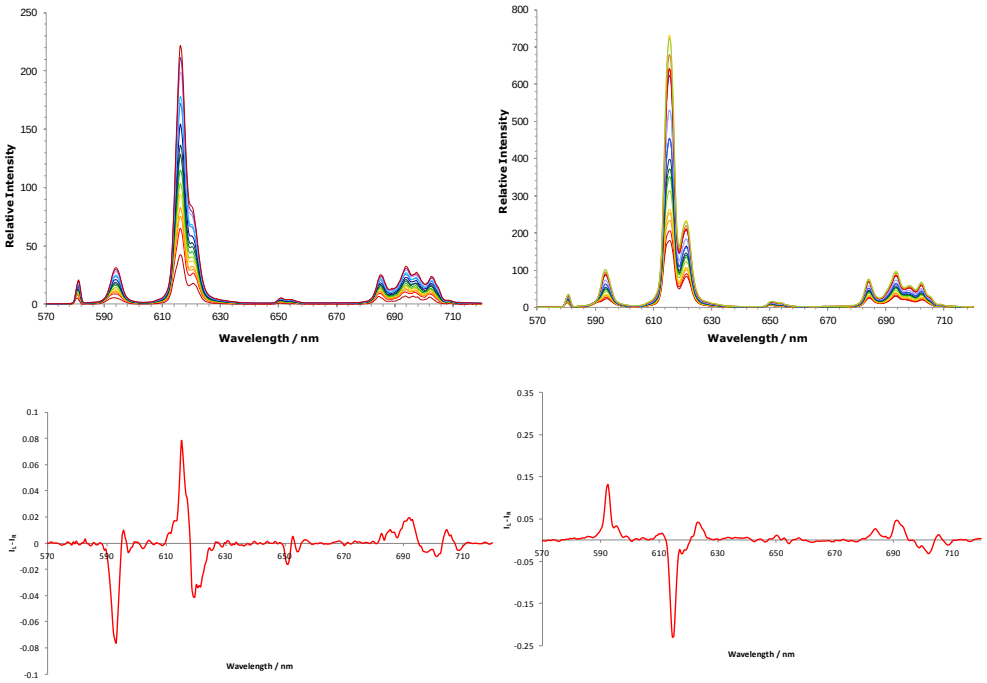

Figure S4 Emission and CPL spectra of [Eu.$\mathbf{L}^{\mathbf{2}}$]$^{3+}$ (*left*) and [Eu.$\mathbf{L}^{\mathbf{3}}$]$^{+}$ (*right*) following addition of 2 mM *R*-lactate (295 K, 10 μM complex, MeOH, effective pH 5.5). Note the different CPL form in the range 580-620 nm and the overall similarity in form, for the 680-720 nm range.

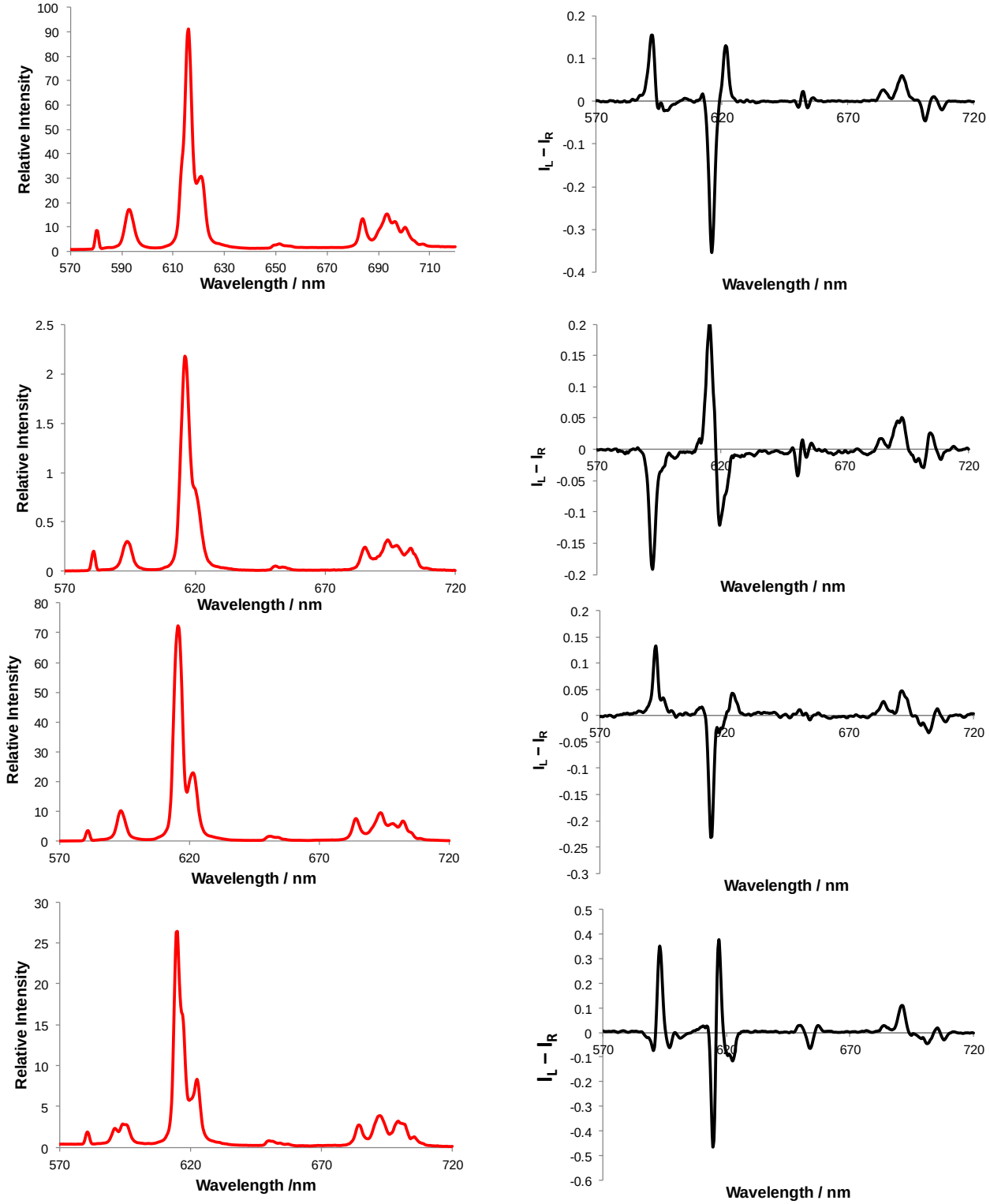

Figure S5 Europium emission (*left*) and CPL (*right*) spectra of Eu(III) complexes of $L^{1\text{-}4}$ (top to bottom respectively) (1:1 v/v aq. MeOH, 10 μM complex, 50 μM *R*-cyclohexylhydroxyacetate, 295K). Note the absence of correlation between adducts of the complexes in the $\Delta J = 1$ and $\Delta J = 2$ CPL transitions, contrasting with the behaviour in the transitions around 680—720 nm. The parent complexes [Eu.$\mathbf{L}^{5\text{-}7}$] (main text) also do not allow correlation of CPL sign with complex helicity in these higher energy transitions between differing donors (amide vs carboxylate vs phosphinate).

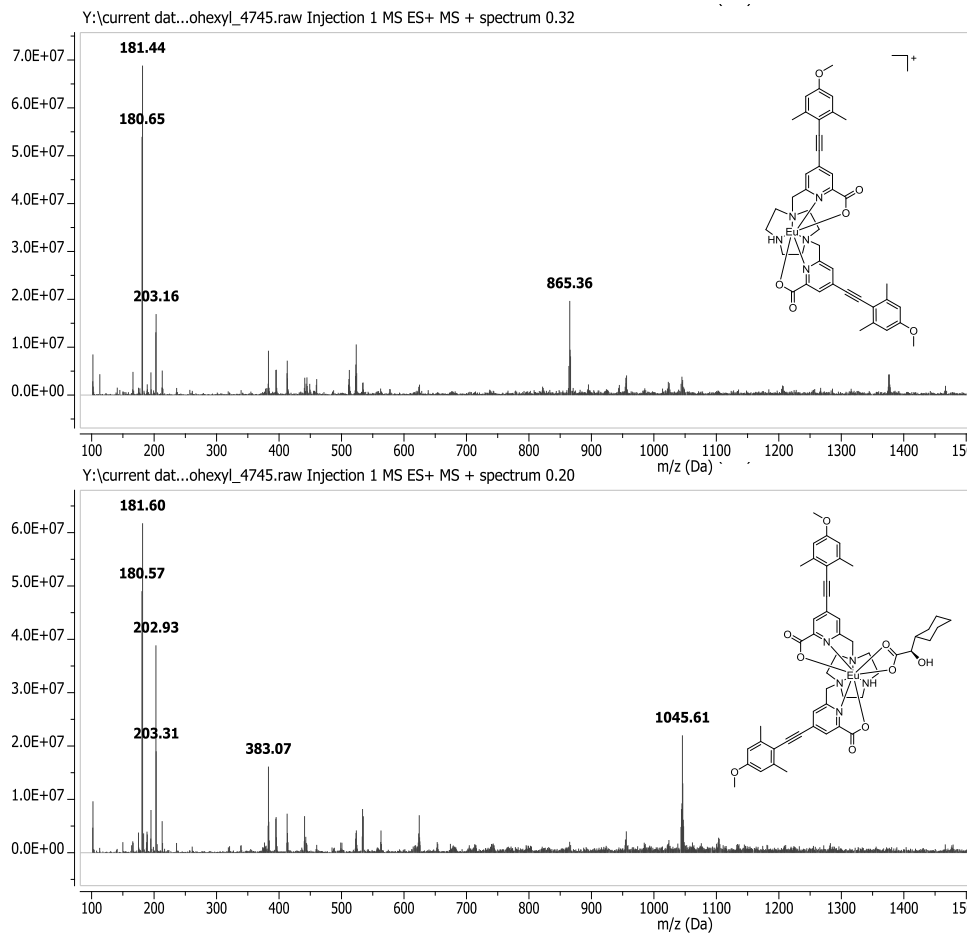

Figure S6 LRMS data for $[Eu.\mathbf{L}^{3}]^{+}$ m/z 865.4 (*top*) and $[Eu.\mathbf{L}^{3}$+cyclohexylhydroxyacetate+Na$]^{+}$ adduct m/z 1045.6 (*bottom*) (ESI no column, MeOH, positive ion mode).

Computations

The model geometries [Y.$\mathbf{L}^{1\text{-}4}$] and adducts in this study were fully optimised without symmetry constraints using the hybrid-DFT B3LYP functional[i] and 3-21G* basis set[ii] for all atoms with the Gaussian 09 package.[iii] Frequency calculations confirmed the geometries to be true minima. The methyl groups at the anisyl groups in [Eu.$\mathbf{L}^{3}$] and [Eu.$\mathbf{L}^{4}$] complexes were omitted in the model geometries [Y.$\mathbf{L}^{3}$] and [Y.$\mathbf{L}^{4}$] to reduce computational effort. Geometry optimisations were also carried out using B3LYP and PBE0 functionals,[i,iv] the SVP basis set[v] and the pseudopotentials, SDD and LANL2DZ,[vi] for comparison with B3LYP/3-21G* and reported X-ray geometries (Tables S1-S3). In all computations, the polarised continuum solvent model (PCM)[vii] with the dielectric constant of water was applied. B3LYP/3-21G* is shown to be an appropriate functional/basis set for Y(III) complexes and therefore suitable models for Eu(III) complexes. The paramagnetic Eu(III) complexes are very difficult to model computationally. Figures of the optimised geometries were generated using Mercury software.[viii]

The benzyl group is assumed to be orientated like the pyridylmethyl groups with respect to the triazacyclononane ligand in all [Y.$\mathbf{L}^{4}$] complexes studied here. For optimised geometries of *R*-lactate bound to the [Y.$\mathbf{L}^{1\text{-}4}$] complexes, intramolecular hydrogen bonds involving the lactate OH group are assumed to be absent as the lactate OH group is likely to be involved in hydrogen bonding with the surrounding solvent molecules. All binding energies were obtained by differences in total energies between metal bound adducts and the corresponding non-metal bound adducts.

(i) (a) A. D. Becke, *J. Chem. Phys.*, 1993, **98**, 5648-5652; (b) C. Lee, W. Yang and R. G. Parr, *Phys. Rev. B*, 1988, **37**, 785-789.

(ii) (a) J. S. Binkley, J. A. Pople and W. J. Hehre, *J. Am. Chem. Soc.*, 1980, **102**, 939-947; (b) M. S. Gordon, J. S. Binkley, J. A. Pople, W. J. Pietro and W. J. Hehre, *J. Am. Chem. Soc.*, 1982, **104**, 2797-2803; (c) W. J. Pietro, M. M. Francl, W. J. Hehre, D. J. Defrees, J. A. Pople and J. S. Binkley, *J. Am. Chem. Soc.*, 1982, **104**, 5039-5048; (d) K. D. Dobbs and W. J. Hehre, *J. Comp. Chem.*, 1986, **7**, 359-378; (e) K. D. Dobbs and W. J. Hehre, *J. Comp. Chem.*, 1987, **8**, 861-879; (f) K. D. Dobbs and W. J. Hehre, *J. Comp. Chem.*, 1987, **8**, 880-893.

(iii) Gaussian 09, Revision A.02, M. J. Frisch, G. W. Trucks, H. B. Schlegel, G. E. Scuseria, M. A. Robb, J. R. Cheeseman, G. Scalmani, V. Barone, B. Mennucci, G. A. Petersson, H. Nakatsuji, M. Caricato, X. Li, H. P. Hratchian, A. F. Izmaylov, J. Bloino, G. Zheng, J. L. Sonnenberg, M. Hada, M. Ehara, K. Toyota, R. Fukuda, J. Hasegawa, M. Ishida, T. Nakajima, Y. Honda, O. Kitao, H. Nakai, T. Vreven, Jr., J. A. Montgomery, J. E. Peralta, F. Ogliaro, M. Bearpark, J. J. Heyd, E. Brothers, K. N. Kudin, V. N. Staroverov, R. Kobayashi, J. Normand, K. Raghavachari, A. Rendell, J. C. Burant, S. S. Iyengar, J. Tomasi, M. Cossi, N. Rega, J. M. Millam, M. Klene, J. E. Knox, J. B. Cross, V. Bakken, C. Adamo, J. Jaramillo, R. Gomperts, R. E. Stratmann, O. Yazyev, A. J. Austin, R. Cammi, C. Pomelli, J. W. Ochterski, R. L. Martin, K. Morokuma, V. G. Zakrzewski, G. A. Voth, P. Salvador, J. J. Dannenberg, S. Dapprich, A. D. Daniels, O. Farkas, J. B. Foresman, J. V. Ortiz, J. Cioslowski and D. J. Fox, *Gaussian, Inc.*, Wallingford CT, **2009**.

(iv) C. Adamo and V. Barone, *J. Chem. Phys.* 1999, **110**, 6158-6169.

(v) (a) A. Schaefer, H. Horn and R. Ahlrichs, *J. Chem. Phys.* 1992, **97**, 2571-2577; (b) A. Schaefer, C. Huber and R. Ahlrichs, *J. Chem. Phys.* 1994, **100**, 5829-5835.

(vi) T. H. Dunning Jr. and P. J. Hay, in *Modern Theoretical Chemistry*, Ed. H. F. Schaefer III, Vol. 3 (Plenum, New York, 1977) 1-28.

(vii) J. Tomasi, B. Mennucci and R. Cammi, *Chem. Rev.* 2005, **105**, 2999-3093.

(viii) C. F. Macrae, I. J. Bruno, J. A. Chisholm, P. R. Edgington, P. McCabe, E. Pidcock, L. Rodriguez-Monge, R. Taylor, J. van de Streek and P. A. Wood, *J. Appl. Cryst.* 2008, **41**, 466–470.

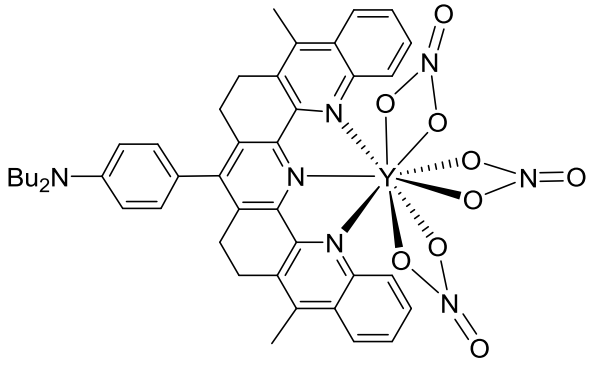

CSD refcode XERTUK

Table S1 Comparison of experimental and computed bond lengths in angstroms for the yttrium complex XERTUK to demonstrate the accuracy of the functional/basis set B3LYP/3-21G*.

	X-ray [a]	B3LYP/3-21G*	PBE0/SDD:SVP	B3LYP/DZP [a]
Y-N	2.364(9)	2.366	2.393	2.477
Y-N	2.503(4)	2.509	2.513	2.638
Y-N	2.518(4)	2.521	2.519	2.638
Y-O	2.443(4)	2.419	2.457	2.385
Y-O	2.360(4)	2.377	2.430	2.385
Y-O	2.387(4)	2.380	2.438	2.428
Y-O	2.431(4)	2.397	2.445	2.428
Y-O	2.454(4)	2.397	2.468	2.440
Y-O	2.429(4)	2.379	2.431	2.440

[a] K. Sénéchal-David, A. Hemeryck, N. Tancrez, L. Toupet, J. A. G. Williams, I. Ledoux, J. Zyss, A. Boucekkine, J.-P. Guegan, H. Le Bozec and O. Maury, *J. Am. Chem. Soc.* 2006, **128**, 12243-12255.

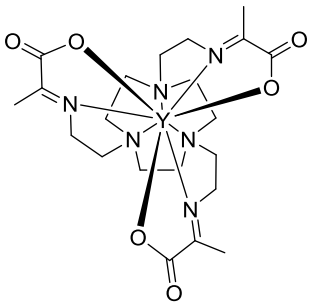

CSD refcode WIWPIB

Table S2 Comparison of experimental and computed bond lengths in angstroms for the yttrium complex WIWPIB to demonstrate the accuracy of the functional/basis set B3LYP/3-21G*.

	X-ray [a]	B3LYP/3-21G*	PBE0/SDD:SVP	B3LYP/DZP
Y-N	2.625(4)	2.604	2.703	2.669
Y-N	2.537(4)	2.566	2.562	2.599
Y-O	2.332(3)	2.298	2.322	2.354

[a] L. Tei, G. Baum, A. J. Blake, D. Fenske and M. Schröder, *J. Chem. Soc., Dalton Trans*. 2000, 2793.

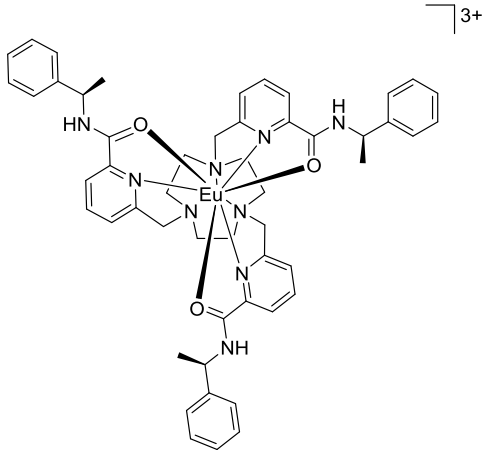

CSD refcode TITQAQ

Table S3 Comparison of experimental and computed bond lengths in angstroms for the europium complex TITQAQ and its model yttrium analogue reflecting the different ionic radii of Eu(III) and Y(III).

	X-ray [a]		B3LYP/3-21G*	Eu-Y difference
Eu-N	2.628(2)	Y-N	2.567	0.061
Eu-N	2.573(2)	Y-N	2.550	0.023
Eu-O	2.405(2)	Y-O	2.357	0.048

[a] E. R. Neil, A. M. Funk, D. S. Yufit and D. Parker, *Dalton Trans*. 2014, **43**, 5490-5504.

Table S4 Water binding energies of [Y.**L**$^{1\text{-}4}$] and radiative rates of decay of the corresponding Eu(III) complexes. The trend reveals binding energies of increasing strength in the order [Y.**L**^{4}]<[Y.**L**^{1}]<[Y.**L**^{3}]<[Y.**L**^{2}].

	Water Binding Energy / kJ mol^{-1}	k (H_2O) / ms^{-1}
[Y.**L**^{1}]	47.5	2.97
[Y.**L**^{2}]	55.6	3.85
[Y.**L**^{3}]	50.8	3.70
[Y.**L**^{4}]	46.4	1.89

Table S5 *R*-Lactate binding energies of [Y.**L**$^{1\text{-}4}$] in Δ configurations and binding constants, log.K, for *R*-lactate complexation of [Eu.**L**$^{1\text{-}4}$]. The trend reveals binding energies of increasing strength in the order [Y.**L**^{1}]<[Y.**L**^{4}]<[Y.**L**^{3}]<[Y.**L**^{2}].

	R-Lactate Binding Energy / kJ mol^{-1}	log$K$ (lactate)
[Y.**L**^{1}]	135.1	2.76
[Y.**L**^{2}]	214.4	4.57
[Y.**L**^{3}]	164.0	4.01
[Y.**L**^{4}]	155.0	3.15

Table S6 Relative water binding energies of *R*-lactate, *R*-mandelate and *R*-cyclohexylhydroxyacetate. The table reveals a trend in hydration binding energies of increasing strength in the order cyclohexylhydroxyacetate < mandelate < lactate.

	Water Binding Energy / kJ mol^{-1}
R-lactate	19.1
R-mandelate	17.2
R-cyclohexylhydroxyacetate	16.5

Table S7 Relative energies in kJ mol^{-1} of the four isomers of [YL-*R*-lactate] adducts.

	L^1	L^2	L^3	L^4
Δ-YL-R-lactate [a]	0	0	0	0
Λ-YL-R-lactate [a]	2.0	0.7	1.5	2.4
Δ-YL-R-lactate [b]	19.5	25.3	27.0	30.3
Λ-YL-R-lactate [b]	21.6	26.7	31.7	36.1

[a] constitution of lactate chelate with lactate carboxylate in same plane as pyridyl N-atoms.

[b] constitution of lactate chelate with lactate OH in same plane as pyridyl N-atoms.

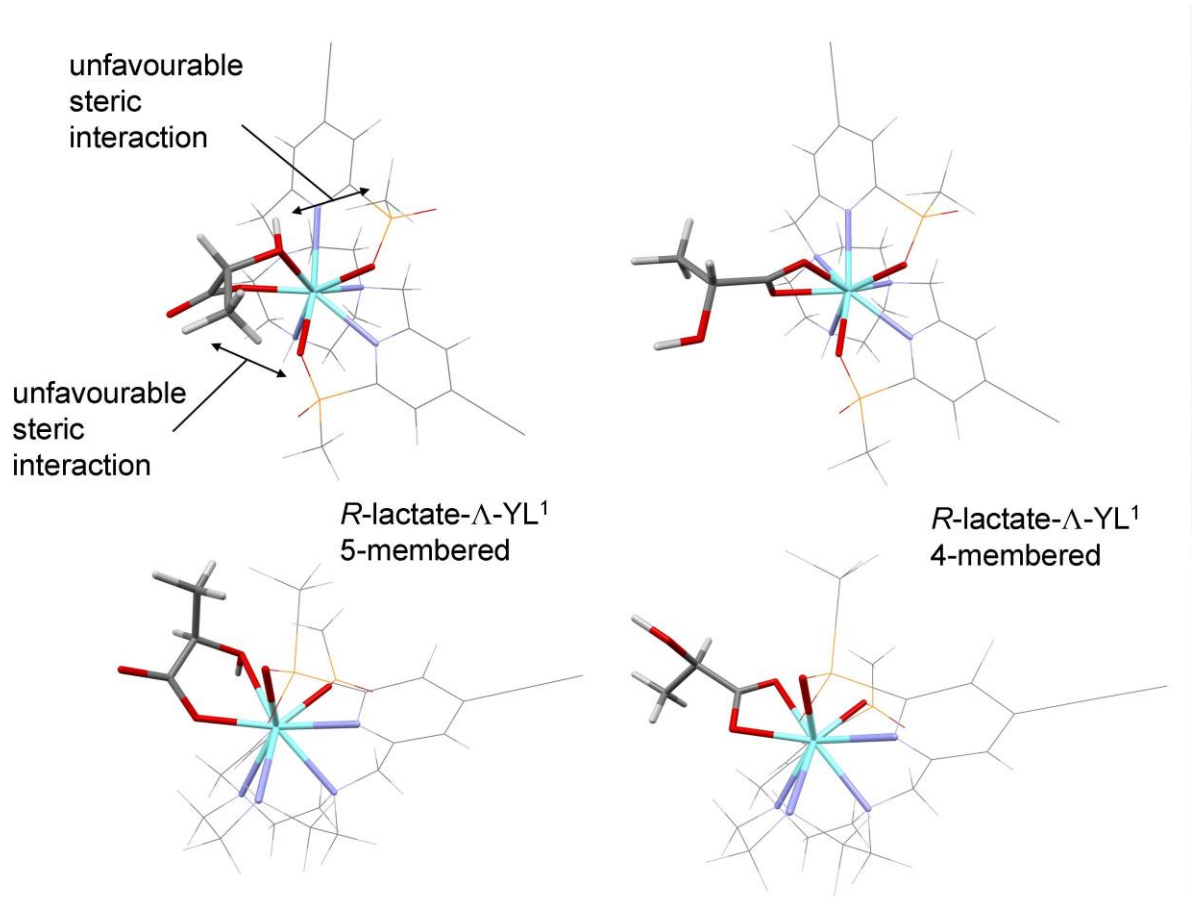

Figure S6. Optimised geometries of [*R*-lactate-Λ-YL^1] with 5- and 4-membered lactate rings. The geometries show the steric effects of the phosphorus arms thus lowering the 5-membered lactate binding strength in [Y.**L^1**] and favouring the 4-membered form suggested for the [Eu**L^1** lactate] complex.

Ligand Synthesis

Dimethyl 4-chloropyridine-2,6-dicarboxylate : *CAS*: 5371-70-0 [1]

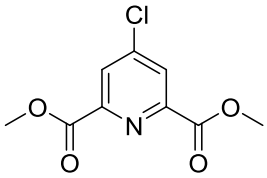

Chelidamic acid (1.00 g, 5.46 mmol) was dissolved in thionyl chloride (5.6 mL) and a few drops of DMF were added. The solution was stirred at 100 °C for 24 h. After complete consumption of the starting material (monitored by LC-MS), the thionyl chloride was removed by vacuum distillation. The residue was dissolved in dry CH_2Cl_2 (3 mL) and cooled to 0 °C. Dry CH_3OH (4 mL) was added dropwise over a period of 10 minutes and the reaction mixture was brought to room temperature. The solvent was removed under reduced pressure and the residue was washed with a saturated sodium bicarbonate solution (40 mL) and extracted into CH_2Cl_2 (3 x 40 mL). The organic layers were combined, washed successively with water (1 x 50 mL) and brine (1 x 50 mL), dried over $MgSO_4$, filtered and the solvent removed under reduced pressure to yield an orange solid (1.196 g, 95%). R_f 0.60 (silica, 5% CH_3OH in CH_2Cl_2); m.p. 141 – 143 °C (lit. 142 °C)[2]; ^{1}H NMR (295 K, 400 MHz, $CDCl_3$) δ_H 8.29 (2H, s, py-H), 4.02 (6H, s, $CO_2C\underline{H}_3$); ^{13}C NMR (295 K, 100 MHz, $CDCl_3$) δ_C 164.2 ($\underline{C}O_2CH_3$), 149.5 (py-C), 146.9 (py-C), 128.4 (py-C), 53.6 ($CO_2\underline{C}H_3$); *m/z* (HRMS$^+$) 230.0216 $[M+H]^+$ ($C_9H_9NO_4Cl$ requires 230.0220).

Dimethyl 4-iodopyridine-2,6-dicarboxylate, *CAS:* 112776-84-8 [1]

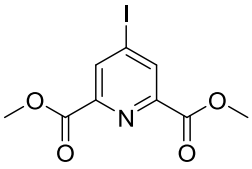

Sodium iodide (3.16 g, 21.1 mmol) was added to a solution of dimethyl 4-chloropyridine-2,6-dicarboxylate (478 mg, 2.11 mmol) in dry acetonitrile (25 mL) and the solution was sonicated (bath sonicator) for 30 min. Acetyl chloride (0.45 mL, 6.33 mmol) was added and the mixture was sonicated for a further 45 min. The solution was washed with sat. Na_2CO_3 (30 mL) and the organic phase separated. The aqueous phase was extracted into CH_2Cl_2 (3 x 25 mL) and the organic layers were combined, washed successively with sat. $Na_2S_2O_3.5H_2O$ (1 x 25 mL), water (1 x 25 mL), dried over $MgSO_4$, filtered, and the solvent removed under vacuum. The crude mixture was purified by flash column chromatography (silica, gradient elution starting from 100% CH_2Cl_2 to 1% CH_3OH in CH_2Cl_2) to yield the compound as a white solid (546 mg, 81%). R_f 0.62 (silica, 5% CH_3OH in CH_2Cl_2); m.p. 179-180 °C (lit. 174-175 °C)[3]; ^{1}H NMR (295 K, 400 MHz, $CDCl_3$) δ_H 8.66 (2H, s, py-

H), 4.02 (6H, s, $CO_2C\underline{H}_3$); ^{13}C NMR (295 K, 100 MHz, $CDCl_3$) δ_C 164.0 ($\underline{C}O_2CH_3$), 148.4 (py-C), 137.3 (py-C), 107.1 (py-C), 53.6 ($CO_2\underline{C}H_3$) ; *m/z* (HRMS$^+$) 321.9569 $[M+H]^+$ ($C_9H_9NO_4I$ requires 321.9576).

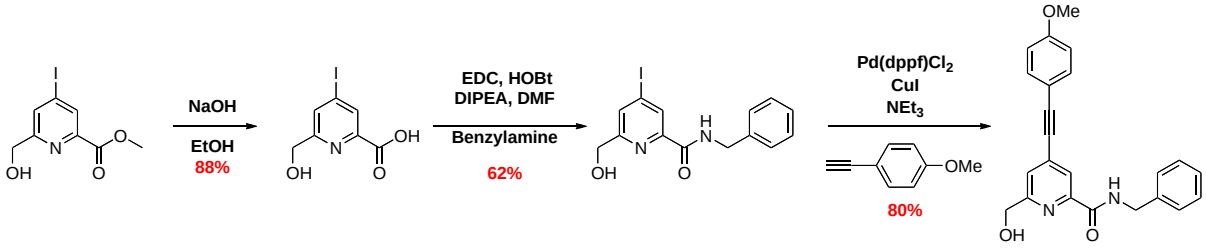

Methyl 6-(hydroxymethyl)-4-iodopicolinate, *CAS:* **1247012-08-3** [4]

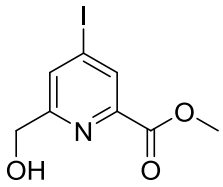

Dimethyl 4-iodopyridine-2,6-dicarboxylate (376 mg, 1.17 mmol) was dissolved in a solution of dry CH_2Cl_2 (3 mL) and dry CH_3OH (2 mL) and cooled to 0 °C. $NaBH_4$ (49 mg, 1.29 mmol) was added to the solution and the reaction was stirred at 0 °C for 1.5 h until complete conversion was observed by TLC. The mixture was quenched with the addition of 1 M HCl (2 mL). The volatile components were removed under vacuum and the aqueous solution was extracted into EtOAc (3 x 25 mL). The organic layers were combined, dried over $MgSO_4$, filtered and the solvent removed under vacuum. The crude solid was purified using flash column chromatography (silica, gradient elution starting from 100% CH_2Cl_2 to 2% CH_3OH in CH_2Cl_2) to give a white solid (247 mg, 72%). R_f 0.27 (silica, 5% CH_3OH in CH_2Cl_2); m.p. 140 – 141 °C; ^{1}H NMR (295 K, 400 MHz, $CDCl_3$) δ_H 8.38 (1H, s, py-H^3), 7.96 (1H, s, py-H^5), 4.81 (2H, s, $C\underline{H}_2OH$), 3.99 (3H, s, $CO_2C\underline{H}_3$); ^{13}C NMR (295 K, 100 MHz, $CDCl_3$) δ_C 164.5 ($\underline{C}O_2CH_3$), 161.2 (C^6), 147.4 (C^2), 133.3 (C$^{3/5}$), 133.2 (C$^{3/5}$), 106.4 (C^4), 64.2 ($\underline{C}H_2OH$), 53.3 ($CO_2\underline{C}H_3$); *m/z* (HRMS$^+$) 293.9630 $[M+H]^+$ ($C_8H_9NO_3I$ requires 293.9627). Found: C, 33.1; H, 2.76; N, 4.80 %. $C_8H_9NO_3I$ requires: C, 32.8; H, 2.75; N, 4.78 %.

6-(Hydroxymethyl)-4-iodopicolinic acid

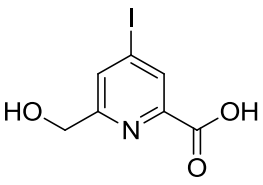

Methyl 6-(hydroxymethyl)-4-iodopicolinate (200 mg, 0.683 mmol) was dissolved in a 1:1 v/v mixture of ethanol:water (6 mL) and NaOH (2 M, 0.5 mL) was added dropwise. The solution was stirred at

room temperature for 1 h. The ethanol was removed under reduced pressure and the aqueous layer was acidified to pH = 4 using a 2 M HCl solution until a white precipitate was formed. The solid was extracted into EtOAc (4 x 50 mL), dried over $MgSO_4$ and concentrated under reduced pressure to yield a white solid (168 mg, 88%) which was used in the next step without further purification. R_f 0.08 (silica, 15% CH_3OH in CH_2Cl_2); m.p. > 190 °C (dec.); ^{1}H NMR (295 K, 400 MHz, MeOD) δ_H 8.38 (1H, s, py-H^3), 8.16 (1H, s, py-H^5), 4.72 (2H, s, py-CH_2); ^{13}C NMR (295 K, 100 MHz, MeOD) δ_C 166 (COOH), 164 (py-C^6), 149 (py-C^2), 134 (py-C^5), 133 (py-C^3), 108 (py-C^4), 64.7 (py-CH_2); *m/z* (HRMS$^+$) 279.9478 $[M+H]^+$ ($C_7H_7NO_3{}^{127}I$ requires 279.9471).

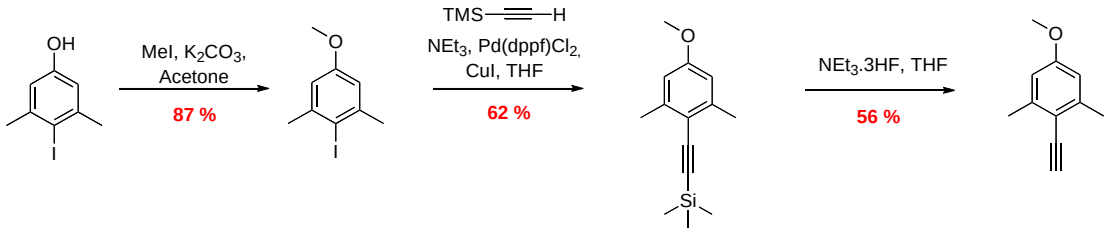

2-Iodo-5-methoxy-1,3-dimethylbenzene: *CAS* **90609-47-5**

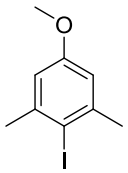

4-Iodo-3,5-dimethylphenol (1.00 g, 4.03 mmol) was dissolved in acetone (10 mL). K_2CO_3 (0.724 g, 5.24 mmol) and iodomethane (0.75 mL, 12.1 mmol) were added and the reaction was heated to reflux and stirred under argon for 24 h. The mixture was filtered to remove the potassium salts and the solvent was removed under vacuum. The residue was dissolved in CH_2Cl_2 (50 mL) and washed with water (50 mL). The aqueous layer was extracted into CH_2Cl_2 (3 x 50 mL) and the organic layers were combined, dried over $MgSO_4$, filtered and the solvent removed under vacuum. The crude solid was purified by flash column chromatography (silica, 2% CH_2Cl_2 in hexane) to a white crystalline solid (1.01 g, 87%). R_f 0.23 (silica, 4% CH_2Cl_2 in hexane); m.p. 36-37 °C (lit. 33-34 °C)[5]; ^{1}H NMR (295 K, 400 MHz, $CDCl_3$) δ_H 6.67 (2H, s, Ar-H), 3.77 (3H, s, O$\underline{C}H_3$), 2.45 (6H, s, $\underline{C}H_3$); ^{13}C NMR (295 K, 100 MHz, $CDCl_3$) δ_C 159.3 (Ar-C^1), 143.0 (Ar-C), 113.0 (Ar-C), 97.2 (Ar-C), 55.4 (O$\underline{C}H_3$), 29.9 ($\underline{C}H_3$); (HRMS+) *m/z* 261.9849 ($C_9H_{11}{}^{127}IO$ requires 261.9855).

1. L. C. Gilday, T. Lang, A. Caballero, P. J. Costa, V. Felix, and P. D. Beer, *Angew. Chem. Int. Ed. Engl.*, 2013, **52**, 4356.

2. Y. Omote, K.-T. Kuo, and N. Sugiyama, *Bull. Chem. Soc. Jpn.*, 1967, **40**, 1695.
3. G. Chessa, L. Canovese, F. Luciano, C. Santo, and R. Seraglia, *Tetrahedron*, 2005, **61**, 1755.
4. A. Bourdolle, M. Allali, J.-C. Mulatier, B. Le Guennic, J. M. Zwier, P. L. Baldeck, J.-C. G. Bunzli, C. Andraud, L. Lamarque, and O. Maury, *Inorg. Chem.*, 2011, **50**, 4987.
5. R. F. C. Brown, F. W. Eastwood and J. M. Horvath, *Aust. J. Chem.*, 1995, **48**, 1055–1058.
6. US Patent: US20100308310A1, 2010.